An Analytical Model for the Interaction between an Insoluble Particle and an Advancing Solid/Liquid Interface

D. SHANGGUAN, S. AHUJA, and D.M. STEFANESCU

In this article, the behavior of particles in front of an advancing solid/liquid interface was analyzed. In the analytical model presented, the critical velocity for the transition from particle pushing to engulfment by the interface was calculated as a function of relevant material parameters and processing variables. In particular, the effect of the difference in the thermal properties of the particle and the matrix on the particle/interface interaction was examined. It was demonstrated that the presence of particles could destabilize the interface which, in turn, affected the behavior of particles at the interface. Based on the analysis, a particle behavior map was constructed to illustrate the complex particle behaviors in different material systems under various growth conditions. Theoretical predictions were compared against experimental results obtained in transparent organic materials as well as in metallic systems. The relevance of these observations to the melt processing of particulate-reinforced metal matrix composites (MMCs) was discussed.

I. INTRODUCTION

THE particle/interface interaction has been a subject of research over the past three decades, due to its relevance to a wide range of phenomena, including particle distribution in ceramic particulate-reinforced metal matrix composites (MMCs),[1] growth of monotectics,[2,3] inclusion segregation in castings,[4] frost heave in soils,[5] and emulsion of organic cell suspensions in ice in cryobiology.[6]

In particulate-reinforced MMCs, *e.g.*, Al/SiC_p, the particle distribution in the matrix is one of the major microstructural features which determines the properties and performance of the composite material produced either by melt processing (MP) or powder metallurgy (PM). In the melt processing of MMCs, the particle distribution is determined by the various interactions involved in the different phases of processing. These include the incorporation of particles into the metallic melt, particle dispersion and particle-particle interaction in the melt, and the interaction between particles and an advancing solid/liquid interface during solidification. In an MMC casting, the first two interactions largely determine the macroscopic distribution of particles in the matrix, while the third primarily determines the microscopic particle distribution, *i.e.*, at the level of grains. The particles can be distributed either uniformly or along grain boundaries, the latter being detrimental to the performance of MMCs. This phenomenon has recently aroused further interest in understanding the interaction between particles and the solid/liquid interface.[1,7–11]

A large number of experimental observations (*e.g.*, References 1, 5, 6, and 8 through 18) have demonstrated that when the interface encounters particles, it can either push them along or engulf them. It has been generally accepted that there exists a critical velocity for the pushing/engulfment transition of particles by an advancing solid/liquid interface. If the interface velocity is below the critical velocity, the particles will be pushed. On the other hand, if the interface velocity exceeds the critical velocity, the particles will be engulfed. Engulfment will normally lead to uniform distribution of particles, while pushing will result in particle segregation. It is thus of great interest to characterize the critical velocity as a function of material parameters and processing variables and ultimately to control particle distribution in the matrix.

Previous studies include experimental measurement of the critical velocity for the pushing/engulfment transition in organic materials,[12–16] water,[12,16–18] and metallic systems.[1,8,9] Theoretical studies[1,8,12,14,17,19–22] have calculated the critical velocity as a function of material parameters and processing variables. It was postulated that[1,19] the difference in the thermal conductivity of the particle and of the matrix may affect the pushing/engulfment transition; however, this was not clearly characterized, and only an empirical relationship was presented.[7] In another work,[21] this consideration was included in a numerical model, but the effect could not be clearly and systematically revealed because of the numerical nature of the work.

This work is a continuation of our efforts in this area and is aimed at refining existing theories on particle pushing/engulfment transition, particularly at characterizing the effect of the difference in the thermal properties of the particle and of the matrix on the behavior of particles at the solid/liquid interface. The theoretical predictions will be compared with available experimental results. The relevance of these observations to the processing of ceramic particulate-reinforced MMCs will be discussed.

II. THEORETICAL ANALYSIS

The objective of the theoretical work was to perform an order of magnitude analysis in order to reveal the dependence of the critical velocity for the pushing/

D. SHANGGUAN, formerly Assistant Research Engineer, The University of Alabama, is now Manufacturing Engineer, Electronics Division, Ford Motor Company, Dearborn, MI 48121. S. AHUJA, Graduate Research Assistant, and D.M. STEFANESCU, University Research Professor, are with the Department of Metallurgical and Materials Engineering, The University of Alabama, Tuscaloosa, AL, 35487-0202.

Manuscript submitted April 5, 1991.

engulfment transition on relevant material parameters and processing variables. Although the analysis deals with a directional solidification configuration, the concept developed can also be instructive while considering equiaxed growth situations which normally occur in castings, as will be discussed later.

In the particle/solid/liquid system under consideration, the solid/liquid interface advances upward, *i.e.*, against gravity, at a steady-state velocity, V. The particle in the melt ahead of the interface experiences the Stokes' flotation due to the gravitational force at the flotation velocity, V_F:

$$V_F = \frac{2}{9}\frac{R^2 \Delta\rho g}{\eta} \qquad [1]$$

with

$$\Delta\rho = \rho_M - \rho_P \qquad [2]$$

where R is the particle radius, g is the gravity level, η is the melt viscosity, and ρ_M and ρ_P are the densities of the melt and of the particle, respectively.

In a vertical growth configuration, depending on the direction and magnitude of the flotation velocity, the particle may either float away from the interface, if $V_F > V$, or approach the interface, if $V_F < V$ or $V_F < 0$ (sedimentation). Therefore, V_F is an interface velocity threshold, that is, only if $V > V_F$ may the particle approach the interface and the particle/interface interaction ever occur.

The following analysis deals with such an interaction. The analysis considers the behavior of a particle in front of a macroscopically planar solid/liquid interface; however, local deviation from planarity will be allowed (Figure 1). This may apply to a configuration where a planar interface is stable or where the particle is very small compared with the scale of the cell or dendrite when cells or dendrites are formed.

The analysis involved the following: (1) solving the temperature field for the particle/matrix configuration; (2) calculating the shape of the solid/liquid interface in the vicinity of the particle, as the interface will locally deviate from planarity if the thermal conductivity of the particle differs from that of the matrix while a macroscopically planar interface may still be maintained; (3) calculating the forces acting on the particle; and (4) establishing the critical condition for the pushing/engulfment transition.

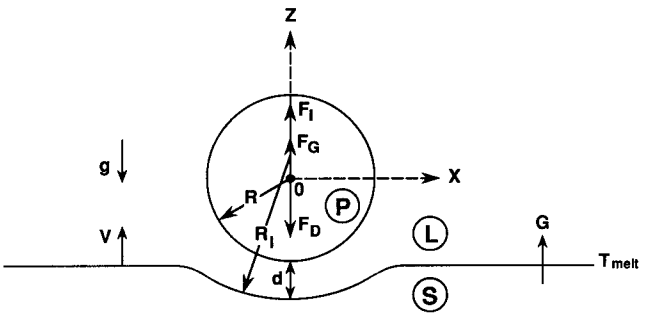

Fig. 1 — Schematic drawing showing a particle in front of the solid/liquid interface and the forces acting on the particle.

A. *The Temperature Field*

In the analysis, heat flow is assumed to be by conduction only; that is, heat transfer by convection and viscous dissipation is neglected. The release of latent heat at the solid/liquid interface is ignored; this, however, can be included in a numerical analysis. As in the case of directional solidification, a temperature gradient, G, is imposed along the growth direction far away from the particle. It is assumed that the solid and liquid phases, *i.e.*, the matrix, have the same thermal conductivity, K_M, which may be different from that of the particle, K_P. The material parameters are assumed to be independent of temperature, and the matrix is assumed to be an isotropic medium.

Assuming azimuthal symmetry, the heat conduction equation in spherical co-ordinates (Figure A1), according to Fourier's law, is given by

$$\frac{1}{r^2}\frac{\partial}{\partial r}\left(r^2\frac{\partial T}{\partial r}\right) + \frac{1}{r^2 \sin\theta}\frac{\partial}{\partial\theta}\left(\sin\theta\frac{\partial T}{\partial\theta}\right) = 0 \qquad [3]$$

The boundary conditions are as follows.

(1) A constant temperature gradient in the Z direction far away from the particle, *i.e.*,

$$\left(\frac{\partial T}{\partial Z}\right)_{r\to\infty} = G \qquad [4]$$

(2) Continuity in temperature across the particle/matrix interface, *i.e.*,

$$(T_M)_{r=R} = (T_P)_{r=R} \qquad [5]$$

where T_M is the temperature in the matrix and T_P is the temperature in the particle.

(3) Intimate contact and no heat accumulation/loss across the particle/matrix interface (*i.e.*, heat flux balance), giving

$$K_M\left(\frac{\partial T_M}{\partial r}\right)_{r=R} = K_P\left(\frac{\partial T_P}{\partial r}\right)_{r=R} \qquad [6]$$

(4) Reference temperature T_0, that is,

$$(T_M)_{Z=0,r\to\infty} = T_0 \qquad [7]$$

It is also assumed that a symmetric boundary condition applies across the Z axis, and that the temparature is finite everywhere in the system. As described in Appendix I, solving Eq. [3] subject to the boundary conditions given by Eqs. [4] through [7] gives the temperature distribution in the matrix, T_M, as well as in the particle, T_P:

$$T_M = T_0 - \left[1 + \frac{1-\alpha}{2+\alpha}\left(\frac{R}{r}\right)^3\right] Gr\cos\theta \qquad [8]$$

$$T_P = T_0 - \left(\frac{3}{\alpha+2}\right) Gr\cos\theta \qquad [9]$$

where α is the thermal conductivity ratio,

$$\alpha = \frac{K_P}{K_M} \qquad [10]$$

Equation [8] is identical to Eq. [23] in Reference 20.

As can be seen, the temperature distribution is a function of the thermal conductivity ratio, α. For $\alpha = 1$, the heat flux lines lie everywhere along the G direction, *i.e.*, the imposed global heat flow direction (the Z direction), and the isotherms, which are perpendicular to the heat flux lines, are everywhere parallel to the X direction. On the other hand, when α differs from 1, in the vicinity of the particle, the isotherms are deflected (Figure 2), reflecting the influence of the difference in the thermal conductivity of the particle and of the matrix on heat flow. For $\alpha < 1$, *i.e.*, the particle has a lower thermal conductivity than the matrix, the heat flux lines diverge from the particle. For $\alpha > 1$, on the other hand, the heat flux lines converge toward the particle.

B. *The Shape of the Solid/Liquid Interface*

The solid/liquid interface is assumed to follow the isotherm for the melting point of the matrix material, T_{melt}; that is, interface undercooling terms are not considered. Assuming that the separation between the particle and the interface at $X = 0$ is d (Figure 1), that is,

$$T_M(X = 0, Z = -(R + d)) = T_{melt} \qquad [11]$$

the isotherm for T_{melt} was shown to be given by (Appendix II):

$$\frac{(R + d)\left(1 + \frac{a}{b}\right)}{r\left[1 + a\left(\frac{R}{r}\right)^3\right]} = \cos\theta \qquad [12]$$

where

$$a = \frac{1 - \alpha}{2 + \alpha} \qquad [13]$$

$$b = \left(1 + \frac{d}{R}\right)^3 \qquad [14]$$

Figures 3 and 4 show interface shapes calculated from Eq. [12]. Figure 3 shows the evolution of the interface as the interface approaches the particle. Figure 4 shows the interface calculated for a number of different thermal conductivity ratios for a fixed d. If the thermal conductivity ratio is unity, a planar interface is maintained. If the thermal conductivity ratio differs from unity, the macroscopically planar interface deviates from planarity behind the particle, the effect becoming more pronounced as the interface approaches the particle. If $\alpha > 1$, a trough is developed on the interface behind the particle, and intuitively, it is expected that this may be conducive to engulfment. On the other hand, if $\alpha < 1$, a bump is developed on the interface behind the particle and pushing is expected to become easier, as the particle may roll down the bump.

The radius of curvature of the interface at $X = 0$, R_I, is calculated to be (Appendix II):

$$R_I = \frac{2a - b}{3a}(R + d) \qquad [15]$$

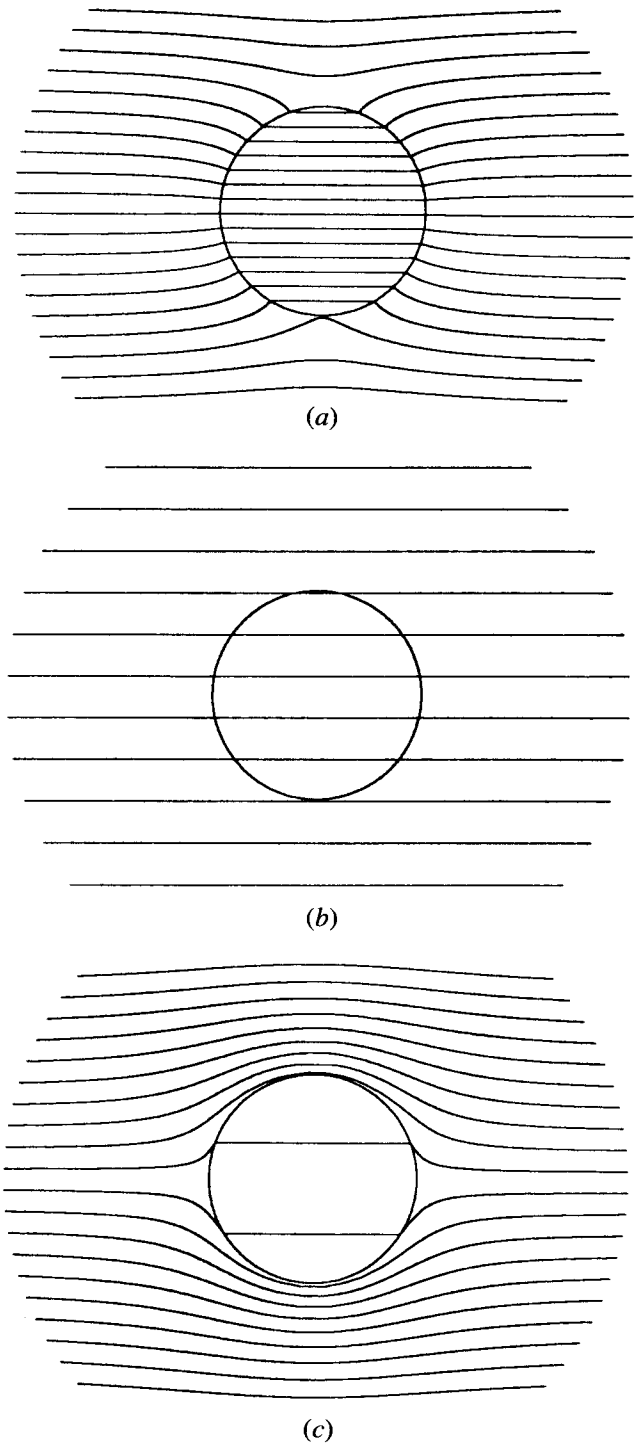

Fig. 2—The calculated isotherms for different thermal conductivity ratios. (*a*) $\alpha = 0.08$; (*b*) $\alpha = 1.0$; and (*c*) $\alpha = 11.1$.

When $d \ll R$,

$$R_I = \frac{2a - 1}{3a}R = \frac{\alpha}{\alpha - 1}R \qquad [16]$$

$$f = \frac{R_I}{R_I - R} = \alpha \qquad [17]$$

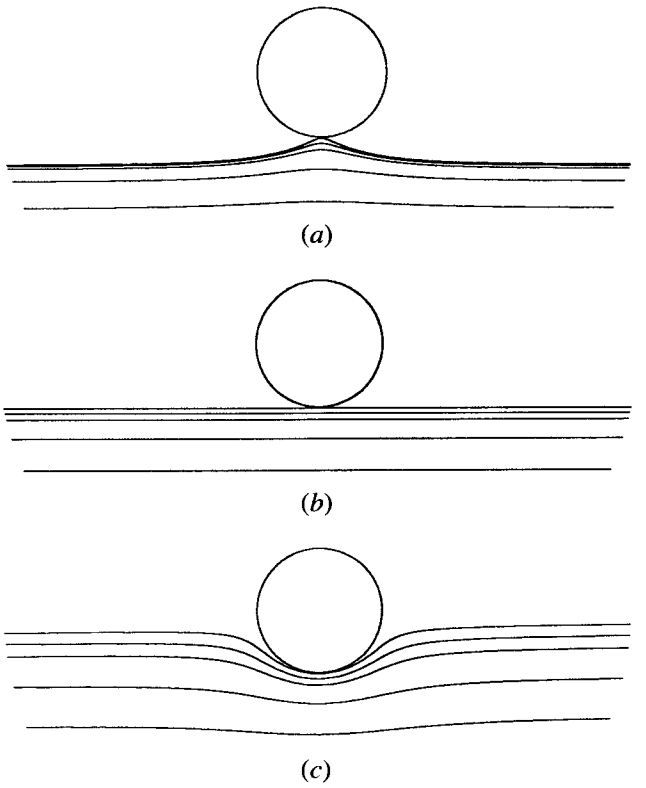

Fig. 3—The evolution of the interface shape as it approaches the particle calculated for different thermal conductivity ratios. (*a*) $\alpha = 0.1$; (*b*) $\alpha = 1.0$; and (*c*) $\alpha = 10.0$.

Analysis of Eq. [16] shows that when $\alpha < 1$, $R_I < 0$ (bump); when $\alpha = 1$, $R_I \to \infty$ (planar); when $\alpha > 1$, $R_I > R$ (trough); and $R_I \to R$ when $\alpha \gg 1$.

C. *Forces Acting on the Particle*

There are three forces acting on the particle (Figure 1): (1) the body force, *i.e.*, the force due to gravity; (2) the drag force, due to flow around the particle which moves along with the interface at V relative to the melt; and (3) the molecular force, *i.e.*, the Van der Waals force, or the force due to the interfacial energy, which occurs as the interface approaches the particle closely enough, *i.e.*, at a distance of the order of the atomic spacing. In the following, these three forces are calculated while the solid/liquid interface, along with the particle, moves upward at the steady-state velocity, V, with the separation between the particle and the interface behind the particle being d (Figure 1). The critical condition for the pushing/engulfment transition will then be established by examining the balance of these forces.

1. *The gravitational force*

The gravitational force, F_G, depends on the density difference between the particle and the melt and the gravity level, g:

$$F_G = \frac{4}{3}\pi R^3 \Delta\rho g \qquad [18]$$

The direction of this force depends on the sign of $\Delta\rho$.

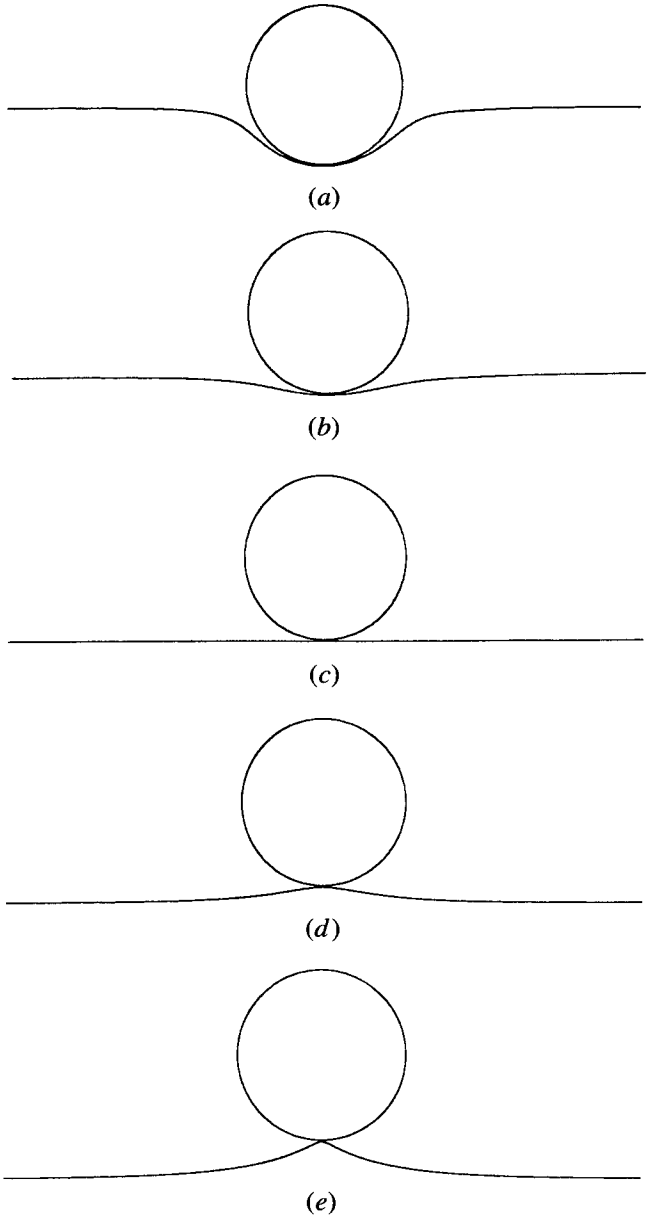

Fig. 4—The calculated interface shapes for different thermal conductivity ratios at a given d. (*a*) $\alpha = 11.1$; (*b*) $\alpha = 2.0$; (*c*) $\alpha = 1.0$; (*d*) $\alpha = 0.5$; and (*e*) $\alpha = 0.06$.

2. *The drag force*

The Stokes' law[23] gives the drag force, F_D, on a sphere which moves relative to the melt at V:

$$F_D = 6\,\pi\eta VR \qquad [19]$$

As a result of the proximity of the interface, the drag force will be affected. For $d \ll R$, following Uhlmann *et al.*[12] and Bolling and Cisse,[19] F_D has been calculated to be:

$$F_D = 6\pi\eta V\,\frac{R^2}{d} \qquad [20]$$

for a planar interface. The detailed mathematics is given in Appendix III based on Bolling and Cissé's approach. For a nonplanar interface, the contribution to the drag

force comes mainly from flow in the particle/interface separation behind the particle. Thus, the drag force can be approximately calculated by assuming the interface to be part of a spherical surface of radius R_I. From Appendix III, the drag force is given by

$$F_D = 6\,\pi\eta V\,\frac{R^2}{d}\left(\frac{R_I}{R_I - R}\right)^2 \qquad [21]$$

From Eq. [17], F_D becomes

$$F_D = 6\pi\eta V\,\frac{R^2}{d}\,\alpha^2 \qquad [22]$$

It can be seen that a concave interface, *i.e.*, $R_I > 0$ as for $\alpha > 1$, results in a greater drag force, while a convex interface, *i.e.*, $R_I < 0$ as for $\alpha < 1$, results in a smaller drag force, as compared with a planar interface.

3. *The force due to the interfacial energy*

The interfacial energies between the solid phase and the liquid phase, between the liquid phase and the particle, and between the solid phase and the particle, are σ_{SL}, σ_{LP}, and σ_{SP}, respectively. Körber *et al.*[18] gave the force due to these interfacial energies, F_I:

$$F_I = 2\pi R\Delta\sigma \qquad [23]$$

This was calculated as the energy required to move the particle over a unit distance into the solid. It may be suggested that[12]

$$\Delta\sigma = \Delta\sigma_0\left(\frac{a_0}{a_0 + d}\right)^n \qquad [24]$$

with $a_0 = r_p + r_s$ = sum of the radii of atoms in the surface layers of the particle and the solid, $n = 2$ through 7 and

$$\Delta\sigma_0 = \sigma_{SP} - \sigma_{LP} - \sigma_{SL} \qquad [25]$$

Then:

$$F_I = 2\pi R\Delta\sigma_0\left(\frac{a_0}{a_0 + d}\right)^n \qquad [26]$$

Potschke and Rogge[20] assumed a nonretarded Van der Waals force between two spheres with radii R and R_I. A modified expression involving the smallest possible distance between the centers of atoms in the solid/liquid interface would be:[20]

$$F_I = 128\pi a_0^2\,\Delta\sigma_0 \cdot \frac{R^3 R_I^3\,(R_I - R - a_0 - d)}{(a_0 + d)^2\,(a_0 + d + 2R)^2\,(a_0 + d - 2R_I)^2\,(a_0 + d - 2R_I + 2R)^2} \qquad [27]$$

If $a_0 + d \ll R$, $a_0 + d \ll R_I$, and $a_0 + d \ll |R_I - R|$, Eq. [27] becomes

$$F_I = 2\pi R\Delta\sigma_0\left(\frac{a_0}{a_0 + d}\right)^2 \frac{R_I}{R_I - R} \qquad [28]$$

For a planar interface, *i.e.*, $R_1 \to \infty$, Eq. [28] becomes equivalent to Eq. [26]. It appears that the force due to the interfacial energy and the molecular force may actually be of the same nature and origin.

From Eq. [17], and generalizing Eq. [28] to include all interactions:

$$F_I = 2\pi R\Delta\sigma_0\left(\frac{a_0}{a_0 + d}\right)^n \alpha \qquad [29]$$

If $\alpha > 1$, a concave interface develops and F_I is increased. If $\alpha < 1$, on the other hand, a convex interface develops and F_I is decreased.

D. *The Critical Condition for the Pushing/Engulfment Transition*

The three forces on the particle play different roles in the pushing/engulfment transition. For upward growth, F_G is conducive to pushing if $\Delta\rho > 0$, F_I is conducive to pushing if $\Delta\sigma_0 > 0$, and *vice versa*, while F_D is always conducive to engulfment. The term F_D is a function of V and d, whereas F_I is a function of d. The equilibrium velocity, V_e, must satisfy the following equation:

$$F_G + F_I - F_D = 0 \qquad [30]$$

i.e.,

$$\frac{4}{3}\,\pi R^3\Delta\rho g + 2\pi R\Delta\sigma_0\left(\frac{a_0}{a_0 + d}\right)^n \alpha - 6\pi\eta V_e\,\frac{R^2}{d}\,\alpha^2 = 0 \qquad [31]$$

Thus,

$$V_e = \frac{d}{3\eta\alpha}\left(\frac{\Delta\sigma_0}{R}\left(\frac{a_0}{a_0 + d}\right)^n + \frac{2R\Delta\rho g}{3\alpha}\right) \qquad [32]$$

If $R \ll R^* = \sqrt{3\Delta\sigma_0\alpha/(8|\Delta\rho|g)}$, F_G is negligible compared with F_I and F_D, and Eq. [32] can be simplified into

$$V_e = \frac{\Delta\sigma_0}{3\eta\alpha}\,\frac{d}{R}\left(\frac{a_0}{a_0 + d}\right)^n \qquad [33]$$

For example, in Al/SiC_p, using the following data ($\Delta\sigma_0$ is estimated, and the other data were taken from Reference 24): $\Delta\sigma_0 = 1$ N/m, $K_M = 93$ W/(mK), $K_I = 85$ W/(mK), $\rho_M = 2700$ Kg/m^3, $\rho_P = 3200$ Kg/m^3, it can be calculated that $\alpha = 0.91$ and $R^* = 8.4$ mm. The particle size in most MMCs is usually 5 to 50 μm, and thus, Eq. [33] is valid for most ceramic particulate-reinforced MMCs.

Maximizing Eq. [33] with regard to d gives the critical distance as:

$$d_C = \frac{a_0}{n - 1} \qquad [34]$$

Then, the critical velocity is:

$$V_C = \frac{a_0}{3\,\eta\alpha(n - 1)}\,\frac{\Delta\sigma_0}{R}\left(\frac{n - 1}{n}\right)^n$$

For $n = 2$, $d_C = a_0$ and

$$V_C = \frac{a_0 \Delta\sigma_0}{12 \eta\alpha R} \quad [34]$$

III. DISCUSSION

A. *Comparison with Experimental and Numerical Results*

In comparing the theoretical prediction of Eq. [34] with experimental results, it is crucial to examine the dependence of V_C on R. Lack of accurate data of $\Delta\sigma_0$, mainly due to unavailability of sensible approaches, either theoretical or experimental, to calculate or measure σ_{SP}, renders it almost impossible at this stage to make a detailed quantitative comparison between theoretical predictions and experimental results for any system. Nonetheless, the predicted dependence of V_C on R generally agrees with experimental findings. Korber *et al.*[18] reported $V_C \alpha 1/R$ in water containing latex particles, while a planar solid/liquid interface was maintained. They observed no compositional dependence of V_C. Fedorov[13] measured V_C in succinonitrile (SCN) and salol containing Ni particles and found $V_C \alpha R^{-4/3}$, again for a planar interface. Omenyi and Neumann[14] reported $V_C \alpha R^{-n}$, with $n = 0.3$ through 1.5, in biphenyl and naphthalene containing acetal and nylon particles. In a number of other material systems, Gilpin[17] and Cisse and Bolling[16] observed that V_C decreased with R, while Uhlmann *et al.*[12] observed that V_C was size-independent for particles smaller than 15 μm and decreased with R for larger ones.

In metallic systems, quantitative measurement is more difficult, and generally, it was observed[1,7,8,25] that V_C decreased with R. The critical velocity for SiC particles in Al matrix predicted by Eq. [34], using $\Delta\sigma_0 = 1$ N/m, $a_0 = 2 \times 10^{-10}$ m, $\eta = 0.005$ PaS, $\alpha = 0.91$, and $R = 2 \times 10$ μm, is 366 μm/s, while it was found in Al-Si/SiC$_p$ castings[26] that SiC particles were pushed at velocities above 100 μm/s. This comparison indicates that the predicted critical velocity is of the same order of magnitude as that found experimentally.

Figure 5 shows a SiC particle being pushed by the solid/liquid interface in SCN. As the thermal conductivity of SiC is higher than that of SCN, a trough is formed on the interface behind the particle, as can be expected from Eq. [16]. The measured critical velocity *vs* particle radius agrees qualitatively with the predicted variation of V_C with R (Figure 6). In this case, Eq. [34] applies, as the growth direction was horizontal, and thus, the gravitational factor did not play a significant role. In calculating V_C, the following estimated data, which are believed to be of the right order of magnitude, were used: $a_0 = 2 \times 10^{-10}$ m, $\eta = 0.001$ PaS, $K_{SiC} = 85$ W/(mK),[24] and $K_{SCN} = 0.15$, giving $\alpha = 567$. Data for $\Delta\sigma_0$ are not available; however, a best fitting between the predicted variation of V_C *vs* R with the experimental curve (Figure 6) suggests $\Delta\sigma_0 = 1.2$ N/m, which is believed to be of the right order of magnitude. A large thermal conductivity ratio, α, is expected to result in $R_I \rightarrow R$, according to Eq. [16], which is consistent with the observed interface shape behind the particle (Figure 5). Details of the experimental work have been published.[27]

Zubko *et al.*[15] studied systematically the effect of the thermal conductivity difference on the pushing/engulfment transition in Zn, Bi, and Sn crystals containing particles of W, Ta, Mo, Fe, Ni, and Cr. They carefully controlled the growth velocity such that a macroscopically planar interface was maintained. Their experimental results showed that in Zn containing W particles, Bi containing W and Ta particles, and Sn containing W and Mo particles, where the particles do not wet the matrix and $K_P/K_M > 1$, engulfment was observed. In Zn containing Ta particles and Sn containing Ta particles, where the particles do not wet the matrix and $K_P/K_M < 1$, pushing was observed. In Sn containing Fe and Ni particles, where the particles wet the matrix and $K_P/K_M > 1$, engulfment was again observed. In Sn containing Cr particles, where the particles wet the matrix and $K_P/K_M < 1$, pushing was observed. These observations convincingly demonstrated the role of the thermal conductivity difference in the pushing/engulfment transition.

In reality, the effect of the thermal conductivity difference may be more pronounced than could be expected from Eq. [34] because of kinetic considerations. For $K_P/K_M < 1$, once a bump is formed on the interface behind the particle, the particle may roll down the bump, making engulfment even more difficult. For $K_P/K_M > 1$,

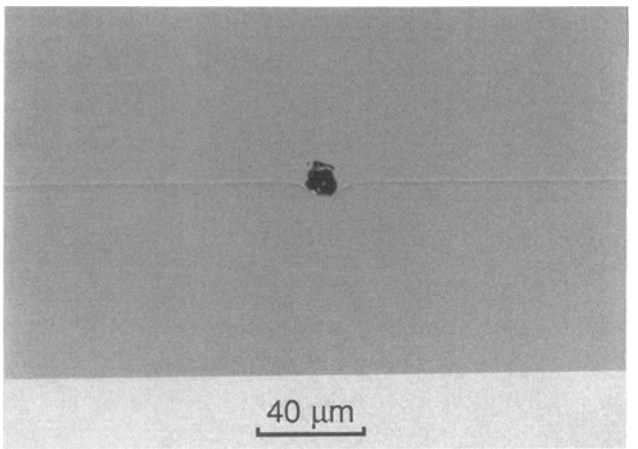

Fig. 5—A SiC particle is being pushed by the solid/liquid interface in SCN.

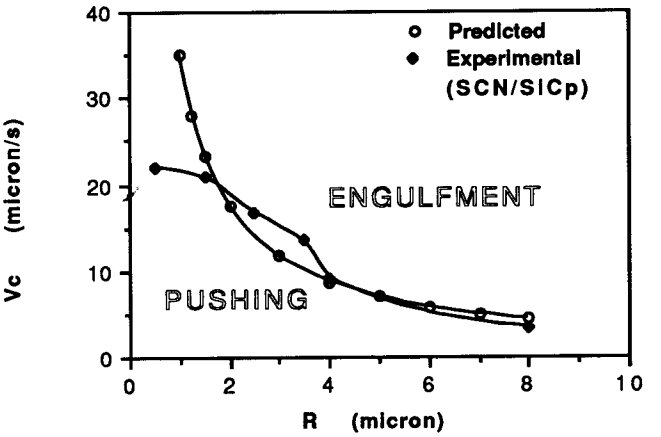

Fig. 6—Comparison of measured and predicted variations of V_C with R for SiC$_p$ in SCN.

once a trough is formed on the interface behind the particle, the interface may grow around the particle, leading to engulfment. This may explain the observations of Zubko *et al.*[15]

The sensitivity of the assumptions made in the analysis could be felt by comparing the analytical result with those obtained by more detailed numerical analyses. Sasikumar *et al.*[21] concluded from their numerical results that $V_C \alpha R^{-1.2}$. Potschke and Rogge[20] presented a rigorous numerical analysis and found that their numerical results could be represented, by means of curve-fitting, by

$$V_C = \frac{a_0 \Delta\sigma_0}{12\eta\alpha} \frac{1}{R} \qquad [35]$$

for a pure material system. Equation [35] is identical to Eq. [34]. These numerical results as well as the experimental results mentioned above all confirm the prediction made by Eq. [34]. The analytical model provides a closed-form expression for the critical velocity and, therefore, can have the advantage of being able to more clearly reveal the roles of various forces in the particle/interface interaction.

B. *A Particle Behavior Map*

A particle behavior map has been proposed[8] and can be used to illustrate the complex particle behaviors in different material systems under various growth conditions. The behavior of particles in front of an advancing solid/liquid interface is determined by Eqs. [1] and [34]. Equation [1] determines whether the interface will ever encounter the particle, depending on the direction and magnitude of V_F relative to V, while Eq. [34] determines whether the particle will be pushed or engulfed if the particle/interface interaction does occur, depending on the magnitude of V relative to V_C.

Figure 7 shows the particle behavior map constructed based on Eqs. [1] and [34], using $a_0 = 2 \times 10^{-10}$ m, $\eta = 0.005$ PaS, $\alpha = 0.91$, $g = 9.81$ m/s^2, $|\Delta\rho| = 500$ Kg/m^3, and $|\Delta\sigma_0| = 1$ N/m. Figures 7(a) and (b) are for growth configurations where the growth direction, $\vec{V}$, is in the same direction as $\vec{V}_F$. This is true for upward growth with $\Delta\rho > 0$ or downward growth with $\Delta\rho < 0$. In this case, the occurrence of the particle/interface interaction depends on the magnitude of V_F as compared to V. Figure 7(a) is for $\Delta\sigma_0 \geq 0$ (nonwetting), which is divided into three regions. If $V < V_F$, the interface will not catch up with the particle; *i.e.*, the particle/interface interaction will occur only if $V \geq V_F$. If $V > V_C \geq V_F$, engulfment is predicted. On the other hand, if $V_C \geq V \geq V_F$, pushing should be expected. The intersection between $V_C(R)$ and $V_F(R)$ is $R' = [3a_0\Delta\sigma_0/(8\Delta\rho g\alpha)]^{1/3} = 25.6$ μm. Figure 7(b) is for $\Delta\sigma_0 < 0$ (wetting), and particle engulfment should be expected as long as the particle/interface interaction occurs ($V \geq V_F$).

Figures 7(c) and (d) are for growth configurations where the growth direction, $\vec{V}$, is not in the same direction as $\vec{V}_F$. This will be true for upward growth with $\Delta\rho \leq 0$ or downward growth with $\Delta\rho \geq 0$. This is also true when the growth direction is horizontal or when the gravity level is low, whatever the sign of $\Delta\rho$. In this case, the particle/interface interaction will always occur. In the case of $\Delta\sigma_0 \geq 0$ (nonwetting), the particle pushing/engulfment transition occurs at V_C (Figure 7(c)). On the other hand, for $\Delta\sigma_0 < 0$ (wetting), particle engulfment should always be expected (Figure 7(d)). A summary of the analysis is presented in Table I.

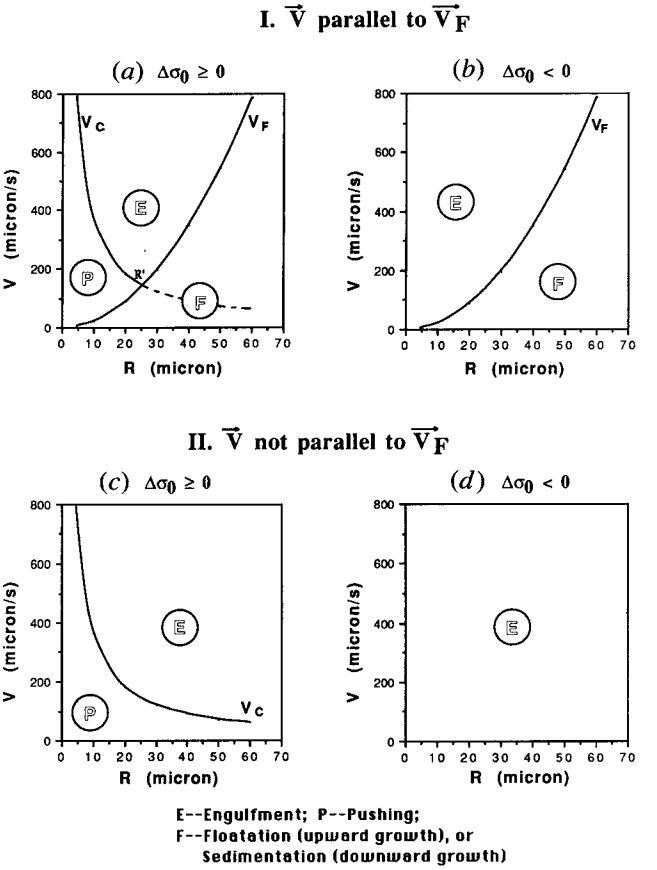

Fig. 7—(*a*) through (*d*) Particle behavior map.

C. *Particle/Interface Interactions*

The analysis presented above has demonstrated that the interaction between particles and the solid/liquid interface is twofold. As the interface approaches the particle, the presence of the particle in front of the interface affects the heat/mass transport in the vicinity of the interface and thus affects the interface shape and its morphological stability. On the other hand, the interface may push or engulf the particle, depending on the balance of forces acting on the particle. In the case of engulfment, solid grows around the particle. If cells or dendrites are formed locally, two or more solidification fronts can converge upon a particle, and eventually, the particle may either be engulfed by one of the fronts or pushed and

Table I. Particle Behavior at the Solid/Liquid Interface

		Growth Direction					
		Upward		Downward		Horizontal (or μ-g)	
$\Delta\rho > 0$	$\Delta\sigma_0 \geq 0$	$V < V_F$	flotation	$V > V_C$	engulfment	$V > V_C$	engulfment
		$V_C > V > V_F$	pushing	$V < V_C$	pushing	$V < V_C$	pushing
		$V_C > V > V_F$	engulfment				
	$\Delta\sigma_0 < 0$	$V > V_F$	engulfment		engulfment		engulfment
		$V < V_F$	flotation				
$\Delta\rho \leq 0$ (or μ-g)	$\Delta\sigma_0 \geq 0$	$V > V_C$	engulfment	$V < V_F$	sedimentation	$V > V_C$	engulfment
		$V < V_C$	pushing	$V_C > V > V_F$	pushing	$V < V_C$	pushing
				$V > V_C > V_F$	engulfment		
	$\Delta\sigma_0 < 0$		engulfment	$V > V_F$	engulfment		engulfment
				$V < V_F$	sedimentation		

eventually entrapped at the end of local solidification in the interdendritic region.

As was stated, the interfacial energy force, F_I, is due to the interfacial energy change, $\Delta\sigma_0$, during the engulfment of the particle into the solid.[20] As shown schematically in Figure 8, $\Delta\sigma_0 = \sigma_2 - \sigma_1 = \sigma_{SP} - (\sigma_{LP} + \sigma_{SL})$, as was given by Eq. [25]. For the interfacial energy force to operate, the separation between the particle and the interface needs to be small enough (the order of the atomic distance, or nanometers). It seems unlikely that F_I will operate at a particle pushing distance of several micrometers, which was used in a numerical calculation.[21]

D. *Particle Distribution in an MMC Casting*

1. *Unidirectional solidification*

Both the experimental results and the theoretical analysis have demonstrated the existence of the critical velocity for the particle pushing/engulfment transition. The concept can be used to interpret the particle distribution in an MMC casting. In unidirectional solidification with a macroscopically planar interface, if the growth rate is below the critical velocity, particles are pushed to the end of the specimen; this may be used advantageously for specimen purification or to achieve controlled particle distribution in gradient materials. If particles are engulfed, the final particle distribution should be unaffected by solidification.

In the case of pushing, particles are built up in front of the solidification front. This will affect the melt viscosity, as given by the relative viscosity, according to Einstein's equation:[28]

$$\eta_r = \eta(1 + 2.5\phi) \qquad [36]$$

where ϕ is the local fraction of particles near the interface. At some stage, the particle buildup may reduce the critical velocity, and engulfment will occur, even if the interface velocity is below the critical velocity calculated for a single particle. As this cycle repeats periodically, bands of particles will appear in the specimen. Therefore, in a casting, at high growth rates, particles are engulfed instantly by the interface, resulting in uniform particle distribution. At intermediate growth rates, particles are pushed for some distance before being engulfed due to particle buildup in front of the interface, resulting in bands of particles. At low growth rates, particles are pushed all the way to the end of the specimen.

The flotation velocity will also be affected by the volume fraction of particles, as given by the reduced flotation velocity,[29] V_r:

$$V_r = V_F(1 - \phi)^{4.65} \qquad [37]$$

A complication in applying the theoretical analysis is particle agglomeration. It has been observed in MMCs that if the wettability between the particle and the matrix melt is poor, particles tend to agglomerate into clusters, normally with a pore at the center of the cluster, in order to reduce the interfacial area between the particle and the matrix. The occurrence of clusters will inevitably affect the critical velocity for pushing/engulfment transition. Moreover, if the particles are attached to a gas pore in the melt, V_F will be different from that calculated from Eq. [1] because of the buoyancy force of the pore. A simple calculation will also show that a less than 3-μm thick gas film around a SiC particle 50 μm in radius will produce enough buoyancy force for the SiC particle to float in Al melt. The thickness required will be even less if the particle has an irregular shape. This may explain why in Al/SiC_p systems, particle flotation is sometimes observed, even though the density of SiC is greater than that of Al.[30]

The analysis was made for a macroscopically planar solidification front. In most cases, however, the growth condition is such that the planar interface is no longer stable, resulting in the formation of cells or dendrites. In fact, the presence of particles may well affect the

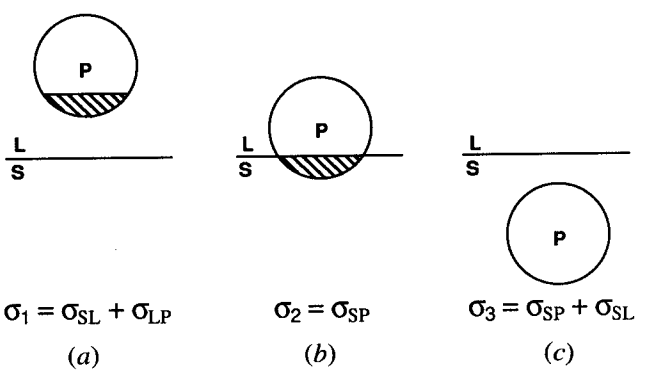

Fig. 8—(*a*) through (*c*) The interfacial energy change during the engulfment of the particle into the solid.

morphological stability of the interface. It is believed that the concept developed in the analysis should still apply for cellular/dendritic interfaces, although some quantitative difference may be expected. If the particle size is small compared to the scale of the local cellular/dendritic front, the local configuration may still be viewed as that depicted in Figure 1. If particles are pushed by a cellular or dendritic interface, the particles will be pushed toward the bulk liquid as well as toward the intercellular/dendritic region and eventually will become entrapped in these regions. Therefore, interdendritic entrapment is actually the consequence of particle pushing.

The analytical expression predicts V_C independent of G. Practically, G affects the morphological stability of the interface and thus ultimately V_C. The shape of particles may also affect the critical velocity.

An irregular particle shape may result in a greater drag force, making the particle more susceptible to engulfment.

2. *Multidirectional solidification*

In a conventional casting, solidification takes place multidirectionally and equiaxed dendritic or eutectic grains normally appear. It is believed that the concept of particle pushing/engulfment should still apply. In this case, particles are either engulfed by the solidification front, resulting in uniform particle distribution, or pushed by the solidification front toward the grain boundaries and eventually entrapped there. The outcome depends on the comparison between the local interface velocity and the critical velocity. The local interface velocity is determined by the local cooling rate. Therefore, it is expected that the pattern of particle distribution will vary with the local casting thickness.

Based on this philosophy, a research program is in progress[7] to model the microstructural evolution through solidification modeling and to incorporate the concept of particle pushing/engulfment transition at the local solidification front across the MMC casting in order to predict the final microstructure map and particle distribution map for an MMC casting.

3. *Controlling particle distribution in an MMC casting*

Situations may arise where it is desirable to have particles in some particular parts of a casting, especially in gradient materials. For example, in an MMC piston, it may be desirable to have particles near its surface in order to improve its wear resistance. In this case, particle pushing may be utilized to push particles to these locations. However, in most applications, a uniform particle distribution is desired, both macroscopically and microscopically. To achieve macroscopically uniform particle distribution, a uniform particle dispersion in the melt is a prerequisite. Stirring, either mechanical or electromagnetic, can be employed to help achieve uniform particle dispersion. To achieve microscopically uniform particle distribution, particles have to be engulfed by the solidification front. A high cooling rate will be beneficial in this regard. Improvement in the wettability between the particle and the melt, either through proper choice of the material system or by matrix alloying or particle surface treatment, will be helpful in preventing particle agglomeration in the melt as well as in achieving particle engulfment instead of pushing. Prediction of particle distribution by computer modeling, as mentioned above, will be a great help in designing MMC castings.

Equation [34] indicates that at a given growth velocity, particles larger than R will be engulfed while those smaller than R will be pushed. This may be used for particle size selection for different parts of an MMC casting.

As mentioned previously, the gravitational force in most cases is unimportant in determining V_C in ceramic particulate-reinforced MMCs. However, due to the existence of the Stokes' force, gravity still plays an important role in particle flotation or sedimentation in the melt, which may result in nonuniform particle dispersion. Furthermore, the direction and magnitude of V_F determines whether the particle/interface interaction will ever occur, as can be seen from Figure 7 and Table I. In this regard, space processing can be used advantageously to eliminate particle flotation or sedimentation in the melt and achieve uniform particle distribution in the matrix.

IV. SUMMARY

An order of magnitude analysis was performed in order to understand the dynamics of an advancing solid/liquid interface behind a particle as well as the behavior of the particle in front of the interface. These two inter-related phenomena constitute the particle/interface interaction. As a result of the particle/interface interaction, there exists a critical velocity for the pushing/engulfment transition of particles by the interface. It was revealed that the critical velocity was a function of a number of material parameters and processing variables, including the melt viscosity, the wettability between the particle and the matrix, the density difference as well as the thermal conductivity difference between the particle and the matrix, the gravity level, and the particle size. Based on the analysis, a particle behavior map was constructed to illustrate the complex particle behaviors in different material systems under various growth conditions. Qualitatively, the theoretical prediction compared favorably with experimental observations. The relevance of the analysis to the processing of ceramic particulate-reinforced MMCs was discussed, and ways of controlling particle distribution in MMC castings were outlined.

APPENDIX I

The temperature field

Equation [3] may be solved by the method of separation of variables (see Figure A1 for coordinate system), assuming

$$T(r,\theta) = R(r)\Theta(\theta) \qquad [Ia]$$

Differentiating Eq. [Ia], substituting into Eq. [3], and multiplying the resultant expression by $(r^2 \sin\theta)/R(r)\Theta(\theta)$ yields

$$\frac{1}{R(r)}\frac{\partial}{\partial r}\left[r^2\frac{\partial R(r)}{\partial r}\right] = -\frac{1}{\Theta(\theta)\sin\theta}\frac{\partial}{\partial\theta}\left(\sin\theta\frac{\partial\Theta(\theta)}{\partial\theta}\right) \qquad [Ib]$$

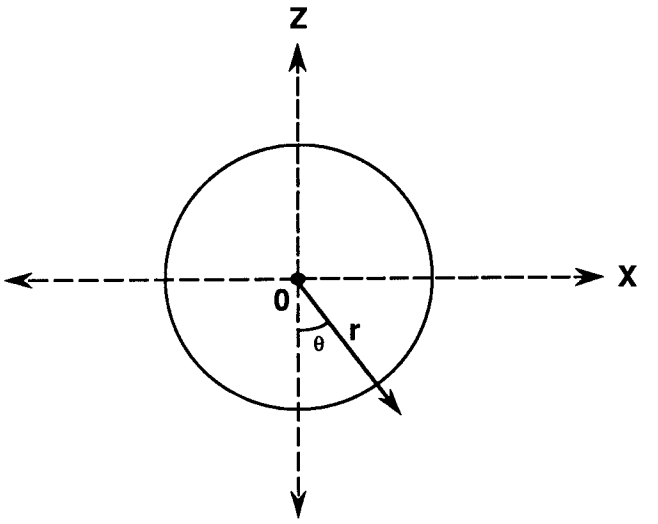

Fig. A1 — The coordinate system used for calculating the temperature field.

Since one side of Eq. [Ib] is independent of the variables on the other side, each side should be equal to a constant, say $n(n+1)$, thus giving

$$\frac{1}{\sin\theta}\frac{\partial}{\partial\theta}\left(\sin\theta\frac{\partial\Theta(\theta)}{\partial\theta}\right) + n(n+1)\Theta(\theta) = 0 \quad [Ic]$$

$$\frac{\partial}{\partial r}\left[r^2\frac{\partial R(r)}{\partial r}\right] - n(n+1)R(r) = 0 \quad [Id]$$

Equation [Ic] is the Legendre's equation, and the solution is given by the Legendre's functions

$$\Theta(\theta) = P_n(\cos\theta) \quad [Ie]$$

Here, $P_n(\cos\theta)$ is the Legendre's polynomial of degree n given by the Rodrigue's formula:

$$P_n(\cos\theta) = \frac{1}{2^n n!}\frac{\partial^n}{\partial(\cos\theta)^n}[(-1)^n\sin^{2n}\theta] \quad [If]$$

Assuming $r = e^s$, differentiating, and substituting into Eq. [Id] gives

$$\frac{\partial^2 R(r)}{\partial s^2} + \frac{\partial R(r)}{\partial s} - n(n+1)R(r) = 0 \quad [Ig]$$

Assuming $R = e^{\beta s}$, differentiating, and substituting into Eq. [Ig] yields

$$(\beta - n)(\beta + n + 1) = 0 \quad [Ih]$$

Thus,

$$\beta = n \quad [Ii]$$

or

$$\beta = -(n+1) \quad [Ij]$$

Therefore, the solution to the radial equation, Eq. [Ig], is

$$R(r) = A_n e^{ns} + B_n e^{-(n+1)s} \quad [Ik]$$

Since $r = e^s$,

$$R(r) = A_n r^n + B_n r^{-(n+1)} \quad [Il]$$

Substituting Eqs. [Ie] and [Il] into Eq. [Ia] gives

$$T(r,\theta) = \sum_{n=0}^{\infty}[A_n r^n + B_n r^{-(n+1)}]P_n(\cos\theta) \quad [Im]$$

Obtaining the coefficients A_n and B_n in Eq. [Im] by applying Eqs. [4] through [7] to Eq. [Im] yields Eqs. [8] and [9].

APPENDIX II

The solid/liquid interface

The solid/liquid interface is assumed to be the isotherm for the melting point, T_{melt}, which is at a distance d below the particle; that is,

$$T_m[X = 0, Z = -(R+d)] = T_{melt} \quad [IIa]$$

From Eq. [8],

$$T_{melt} = T_0 - G(R+d)\left(1 + \frac{a}{b}\right) \quad [IIb]$$

$$T_0 = T_{melt} + G(R+d)\left(1 + \frac{a}{b}\right) \quad [IIc]$$

where a and b are defined by Eqs. [13] and [14], respectively. Again, from Eq. [8], the melting isotherm must satisfy

$$\cos\theta = \frac{T_0 - T_{melt}}{Gr\left[1 + a\left(\frac{R}{r}\right)^3\right]} \quad [IId]$$

Substituting Eq. [IIc] into Eq. [IId] yields

$$\cos\theta = \frac{(R+d)\left[1 + \frac{a}{b}\right]}{r\left[1 + a\left(\frac{R}{r}\right)^3\right]} \quad [IIe]$$

Equation [IIe] is the equation for the interface. At the center of the interface, *i.e.*, $r = R + d$ and $\theta = 0$,

$$\frac{\partial r}{\partial\theta} = 0 \quad [IIf]$$

$$\frac{\partial^2 r}{\partial\theta^2} = \frac{b+a}{b-2a}(R+d) \quad [IIg]$$

By definition,

$$R_I = \frac{\left[r^2 + \left(\frac{\partial r}{\partial\theta}\right)^2\right]^{3/2}}{r^2 + 2r\frac{\partial r}{\partial\theta} - r\frac{\partial^2 r}{\partial\theta^2}} \quad [IIh]$$

$$R_I = \frac{2a-b}{3a}(R+d) \quad [IIi]$$

APPENDIX III

The drag force

As shown in Figure A2, the particle/interface separation, h, is given by

$$h = d + R - \sqrt{R^2 - X^2} - H(X) \qquad \text{[IIIa]}$$

Following Bolling and Cisse,[19] the velocity profile, U, for the fluid flow through the interface/particle separation is assumed to be

$$U = C(X)\,[h - Z' + H(X)]\,[Z' - H(X)] \qquad \text{[IIIb]}$$

where $Z' = Z + (R + d)$. Equation [IIIb] satisfies the boundary conditions

$$U[Z' = H(X)] = 0 \qquad \text{[IIIc]}$$

$$U[Z' = H(X) + h] = 0 \qquad \text{[IIId]}$$

Mass conservation requires

$$-\int_{H(X)}^{h+H(X)} 2\pi X U\, dZ' = \pi X^2 V \qquad \text{[IIIe]}$$

Solving Eq. [IIIe] yields

$$C(X) = -\frac{3XV}{h^3} \qquad \text{[IIIf]}$$

Neglecting $\partial U/\partial X$ and $\partial^2 U/\partial X^2$ as they are small compared with $\partial^2 U/\partial Z^2$ yields

$$\frac{\partial P}{\partial X} = \eta \frac{\partial^2 U}{\partial Z^2} \qquad \text{[IIIg]}$$

Thus,

$$\frac{\partial P}{\partial X} = \frac{6\eta X V}{h^3} \qquad \text{[IIIh]}$$

$$P(R) - P(X) = \int_X^R \frac{\partial P}{\partial X}\, dX = \int_X^R \frac{6\eta X V}{h^3}\, dX \qquad \text{[IIIi]}$$

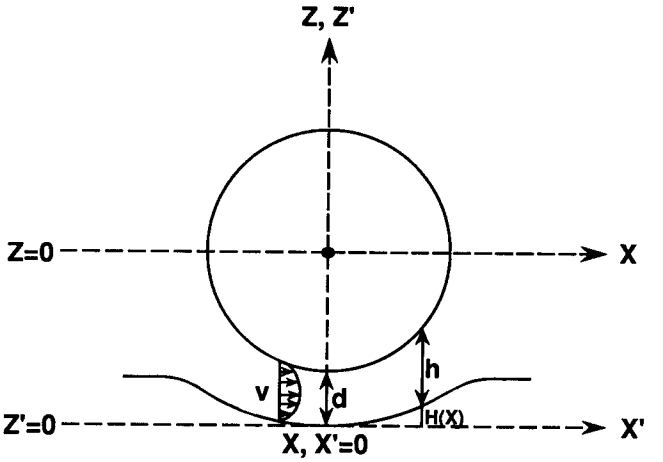

Fig. A2—Symbols and the coordinate system used in the calculation of the drag force.

The drag force, therefore, is

$$F_D = \int_0^R 2\pi X[P(R) - P(X)]\, dX$$

$$= \int_0^R 2\pi X \int_X^R \frac{6\eta V}{h^3}\, \xi d\xi\, dX$$

$$= 12\pi\eta V \int_0^R X \int_X^R \frac{\xi}{h^3}\, d\xi\, dX \qquad \text{[IIIj]}$$

For a planar interface,

$$H(X) = 0 \qquad \text{[IIIk]}$$

$$h = d + R - \sqrt{R^2 - X^2}$$

$$\approx d + \frac{X^2}{2R} \qquad \text{[IIIl]}$$

as

$$R - \sqrt{R^2 - X^2} \approx \frac{X^2}{2R} \quad \text{for } R \gg X \qquad \text{[IIIm]}$$

Thus,

$$F_D = 6\pi\eta V R \frac{R^3}{4d(d + R/2)^2} \qquad \text{[IIIn]}$$

For $d \ll R$,

$$F_D = 6\pi\eta V \frac{R^2}{d} \qquad \text{[IIIo]}$$

For a spherical interface with radius R_I,

$$h = d + R - \sqrt{R^2 - X^2} - R_I + \sqrt{R_I^2 - X^2}$$

$$\approx d + \frac{X^2}{2}\left(\frac{1}{R} - \frac{1}{R_I}\right) \quad \text{for } R \gg X,\ R_I \gg X \qquad \text{[IIIp]}$$

It can then be shown that

$$F_D = 6\pi\eta V \frac{R^2}{d}\left(\frac{R_I}{R_I - R}\right)^2 \qquad \text{[IIIq]}$$

LIST OF SYMBOLS

F_D	drag force
F_G	gravitational force
F_I	force due to interfacial energies
G	temperature gradient
$H(X)$	interface shape function
K_P	thermal conductivity (particle)
K_M	thermal conductivity (matrix)
P	hydrodynamic pressure
R	particle radius
R_I	interface radius
T	temperature
T_P	temperature in the particle
T_M	temperature in the matrix
T_{melt}	matrix melting temperature
T_0	reference temperature
U	flow velocity

V	interface velocity
V_C	critical velocity
V_e	equilibrium velocity
V_F	flotation velocity
a_0	atomic distance
d	particle/interface separation behind the particle
g	gravity
h	particle/interface separation
α	thermal conductivity ratio
η	melt viscosity
η_r	relative melt viscosity
ϕ	particle volume fraction
ρ_P	particle density
ρ_M	melt density
$\Delta\rho$	density difference
σ_{SP}	solid/particle interfacial energy
σ_{SL}	solid/liquid interfacial energy
σ_{LP}	liquid/particle interfacial energy
$\Delta\sigma_0$	interfacial energy difference

Subscripts

I	interface
L	liquid
M	matrix
P	particle
S	solid

ACKNOWLEDGMENTS

This work was partially supported by the Alabama Research Institute under Grant No. ARI 89-301. Dr. G. Kaptoy's contribution to the clarification of some of the issues related to the interfacial force is greatly appreciated.

REFERENCES

1. D.M. Stefanescu, B.K. Dhindaw, S.A. Kacar, and A. Moitra: *Metall. Trans. A*, 1988, vol. 19A, pp. 2847-55.
2. B.K. Dhindaw, D.M. Stefanescu, A.K. Singh, and P.A. Curreri: *Metall. Trans. A*, 1988, vol. 19A, pp. 2839-46.
3. N.L. Frier, Y. Shiohara, and K.C. Russell: in *Materials Research Society International Meeting on Advanced Materials, MRS*, 1989, vol. 4, pp. 47-52.
4. M.C. Flemings: *Solidification Processing*, McGraw-Hill, New York, NY, 1974.
4. M.C. Flemings: *Solidification Processing*, McGraw-Hill, New York, NY, 1974.
5. A.E. Corte: *J. Geophys. Res.*, 1962, vol. 67 (3), pp. 1085-90.
6. V.L. Brostein, Y.A. Itkin, and G.S. Ishkov: *J. Cryst. Growth*, 1981, vol. 52, pp. 345-49.
7. D. Shangguan and D.M. Stefanescu: in *Proc. XXII ICHMT Int. Symp. on Manufacturing and Materials Processing*, Dubrovnik, Yugoslavia, Aug. 1990, in press.
8. D.M. Stefanescu, A. Moitra, A.S. Kacar, and B.K. Dhindaw: *Metall. Trans. A*, 1990, vol. 21A, pp. 231-39.
9. B.K. Dhindaw, A. Moitra, D.M. Stefanescu, and P. Curreri: *Metall. Trans. A*, 1988, vol. 19A, pp. 1899-1904.
10. D.M. Stefanescu and F. Rana: in *Microstructural Development and Control in Materials Processing*, D.R. Durham and A. Saigal, eds., ASME, Fairfield, NJ, 1989, pp. 95-102.
11. D. Shangguan and D.M. Stefanescu: *Metall. Trans. B*, 1991, vol. 22B, pp. 385-88.
12. D.R. Uhlmann, B. Chalmers, and K.A. Jackson: *J. Appl. Phys.*, 1964, vol. 35 (10), pp. 2986-93.
13. O.P. Fedorov: *J. Cryst. Growth*, 1990, vol. 102, pp. 857-61.
14. S.N. Omenyi and A.W. Neumann: *J. Appl. Phys.*, 1976, vol. 47 (9), pp. 3956-62.
15. A.M. Zubko, V.G. Lobanov, and V.V. Nikonova: *Sov. Phys.—Crystallogr.*, 1973, vol. 18 (2), pp. 239-41.
16. J. Cisse and G.F. Bolling: *J. Cryst. Growth*, 1971, vol. 11, pp. 25-28.
17. R.R. Gilpin: *J. Colloid Interface Sci.*, 1980, vol. 74 (1), pp. 44–63.
18. Ch. Korber, G. Rau, M.D. Cosman, and E.G. Cravalho: *J. Cryst. Growth*, 1985, vol. 72, pp. 649-62.
19. G.F. Bolling and J.A. Cisse: *J. Cryst. Growth*, 1971, vol. 10, pp. 56-66.
20. J. Potschke and V. Rogge: *J. Cryst. Growth*, 1989, vol. 94, pp. 726-38.
21. R. Sasikumar, T.R. Ramamohan, and B.C. Pai: *Acta Metall.*, 1989, vol. 37 (7), pp. 2085-91.
22. A.A. Chernov, D.E. Temkin, and A.M. Mel'nikova: *Sov. Phys.—Crystallogr.*, 1976, vol. 21 (4), pp. 369-73.
23. R.B. Bird, W.E. Stewart, and E.N. Lightfoot: *Transport Phenomena*, John Wiley & Sons, New York, NY, 1960.
24. *Handbook of Chemistry and Physics*, 67th ed., CRC Press, Boca Raton, FL, 1986.
25. I. Jin and D.J. Lloyd: in *Proc. Int. Conf.*, Montreal, PQ, Canada, September 17–29, 1990, J. Masounave and F.G. Hamel, eds., ASM INTERNATIONAL, Metals Park, OH, 1990.
26. D.J. Lloyd: *Compos. Sci. Technol.*, 1989, vol. 35, pp. 159-79.
27. S. Ahuja, D. Shangguan, and D.M. Stefanescu: in *Advanced Metal Matrix Composites for Elevated Temperatures*, ASM Conference Proceedings, Cincinnati, OH, October 20–24, 1991, pp. 205-12.
28. D.J. Jeffrey and A. Acrivos: *J. Amer. Inst. Chem. Eng.*, 1976, vol. 22 (3), pp. 417-32.
29. J.F. Richardson and W.N. Zaki: *Chem. Eng. Sci.*, 1954, vol. 3, pp. 65-73.
30. X. Guo, D. Shangguan, and D.M. Stefanescu: The University of Alabama, Tuscaloosa, AL, unpublished research, 1991.